applied sciences

MDPI

Article

A Two-Stage Damage Localization Method for Structural Sealants Based on Boundary Modal Curvature

Xichen Zhang [1], Kun Jiang [2], Danguang Pan [2,*], Xiangqiu Fu [1] and Naidong Hu [1,2]

[1] State Key Laboratory of Building Safety and Environment, China Academy of Building Research, Beijing 100013, China; zhangxichen@cabr-bctc.com (X.Z.); fuxiangqiu@cabr-bctc.com (X.F.); hunaidong@cabr-bctc.com (N.H.)
[2] Department of Civil Engineering, University of Science and Technology Beijing, Beijing 100083, China; d202110016@xs.ustb.edu.cn
* Correspondence: pdg@ustb.edu.cn; Tel.: +86-139-1162-3597

Abstract: To facilitate the maintenance of hidden frame glass curtain walls, it is necessary to identify the damage location of the structural sealant accurately. However, detecting concealed sealant damage directly is challenging. This paper proposes a two-stage damage localization method to pinpoint the center of damaged structural sealants. In the first stage, an assurance criterion of boundary modal curvature (ACBMC) is developed to identify damaged edges. In the second stage, the exact damage location is determined by comparing the differences in boundary modal curvature between the undamaged and damaged edges. Two-panel units are analyzed by numerical and model experiments. The results show that the proposed method can effectively identify the damage location of the structural sealant when the damage severity is higher than 4%.

Keywords: damage localization; two-stage method; structural sealant; boundary mode; mode curvature

check for updates

Citation: Zhang, X.; Jiang, K.; Pan, D.; Fu, X.; Hu, N. A Two-Stage Damage Localization Method for Structural Sealants Based on Boundary Modal Curvature. *Appl. Sci.* **2024**, *14*, 9641. https://doi.org/10.3390/app14219641

Academic Editor: Eleni Tsangouri

Received: 13 September 2024
Revised: 18 October 2024
Accepted: 19 October 2024
Published: 22 October 2024

Copyright: © 2024 by the authors. Licensee MDPI, Basel, Switzerland. This article is an open access article distributed under the terms and conditions of the Creative Commons Attribution (CC BY) license (https://creativecommons.org/licenses/by/4.0/).

1. Introduction

A hidden frame glass curtain wall (HFGCW) is a key component of modern architecture, primarily composed of a structural sealant, glass panel, and supporting frame. In the service process, the structural sealant would be damaged [1–3], which poses a risk for maintenance and potential accidents such as glass panel detachment.

The damage location identification methods of structural sealants can be mainly classified as destructive and non-destructive detection methods [4,5]. Destructive detection methods, such as the balloon method and the suction cup method [6–10], involve dismantling decorative cover plates to directly inspect the structural sealant. These methods can provide detailed information about the damage location of the structural sealant. However, it would destroy the sample and is only suitable for small-scale testing of a limited number of panel units.

Non-destructive detection methods allow for identifying the defects without removing the decorative cover plate. Common non-destructive testing methods include dynamic-based testing, ultrasonic testing, X-ray testing, infrared testing, etc. [11–13]. Ultrasonic testing has real-time capability, but it is not intuitive; the detection results are easily affected by subjective and objective factors. X-ray testing and infrared testing can accurately pinpoint the damage and location, but they can only detect surface defects and cannot identify hidden damages. Based on the characteristics of being global and fast, the dynamic method is widely used in detecting damage in bridges and structures [14,15]. Changes in the modal parameters and dynamic response between the undamaged and damaged panel units are often used to identify the damage to structural sealants. Huang et al. [16–18] detected the damage to the structural sealant by comparing the measured natural frequencies and theoretic ones. However, natural frequencies provide only overall characteristics and lack specific damage location information. Recently, dynamic responses, which contain

responses of higher modes, were used to identify the damage. Pan et al. [19] utilized the difference in frequency response function to identify the damage to structural sealant. Jiang et al. [20] proposed the statistical baseline model to identify the damage to structural sealant. Yang et al. [21] proposed the wavelet transform method to identify the damage to structural sealant. By analyzing the changes in the response of the glass panel, the changing of state of the glass panel can be analyzed to further identify the damage to the structural sealant [22–25].

To identify the damage location of structural sealants, the modal characteristics are a potential indicator. Liu et al. [26,27] demonstrated that changes in vibration modes could be used to identify damage. Fang and Luo [28] calculated the curvature mode difference in the glass panel to identify the damage location of the structural sealant. To identify the structural sealant damage on the boundary, Jiang et al. [29] introduced the variation in the average boundary mode assurance criterion (BMAC), the average difference in the boundary modal curvature, and the average boundary mode strain energy with the increase in the damage severity of structural sealant. The testing results show that these damage identification methods based on boundary modes can identify the damaged edge of structural sealant, but cannot determine the exact location of the damage. According to the current study, it is a challenge to point out the specific damage location of structural sealant.

The aim of this paper is to develop a two-stage damage localization method to identify the exact damage location of structural sealant. In the first stage of such an identification method, the concept of assurance criterion of boundary modal curvature (ACBMC) is proposed. Then, the damaged edges are identified using the ACBMC. In the second stage, the damage location is further identified by comparing the difference in boundary modal curvature (BMC). Firstly, two panel units with different sizes were investigated by numerical test. Considering the influence of the damage severity and measurement noise, a threshold of damage identification on the ACBMC is proposed. Then, model tests were carried out on the two panel units. Both numerical and experimental results demonstrate that the proposed method effectively identifies the damage location of structural sealants.

2. Basic Theory

2.1. BMC of Glass Panels

Figure 1 shows the model of a panel unit in HFGCW, which consists of a glass panel, structural sealant, and supporting frame. A structural sealant is an elastic material that be located at four edges of the glass panel. When the panel unit is meshed using the finite element method, the equation of motion governing the free vibration of the panel unit can be expressed as

$$([K] - \omega^2[M])\{\varphi\} = \{0\} \tag{1}$$

where the ω is the natural frequency of the panel unit and $[K]$ and $[M]$ are the stiffness matrix and mass matrix, respectively. The stiffness and mass matrix consists of a glass panel, structural sealant, and supporting frame. $\{\varphi\}$ is the mode shape of the glass panel.

The damage of glass panels is easily detected visually. The concealed damages were mainly located at the structural sealant. When the structural sealant is damaged, the changes in the mode of the glass panel are not obvious. To highlight mode variations after sealant damage, the mode displacements along the panel's boundary, referred to as boundary modes, are analyzed. The four edges are called as a, b, c and d, respectively. Then, the boundary mode i can be expressed as $\{\varphi_i^r\} = \left\{\varphi_{1,i}^r \quad \varphi_{2,i}^r \quad \cdots \quad \varphi_{n_r,i}^r\right\}^T$ (r = a, b, c, d). n_r is the total number of measurement points on the r-th edge.

For each edge, the BMC are computed from the boundary mode using the central difference approximation for mode i and measured point j, as follows:

$$C_{j,i}^r = \frac{\varphi_{j-1,i}^r - 2\varphi_{j,i}^r + \varphi_{j+1,i}^r}{h^2} \tag{2}$$

where h is the length between the two measurement points.

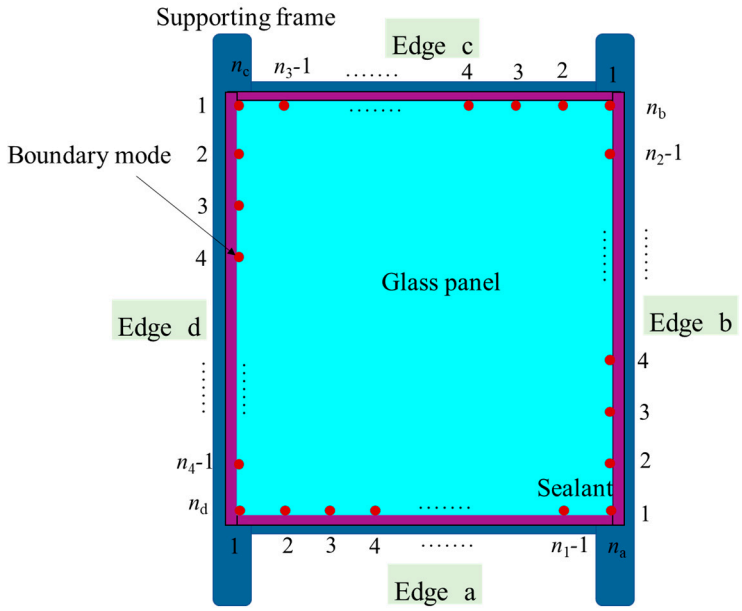


Figure 1. Boundary mode of glass panel.

2.2. The First Stage on Damaged Edge Identification

Assuming that damage to the structural sealant does not cause a change in the structural mass, the obtained displacement modes are orthogonally normalized with respect to the mass matrix. When the structural sealant is damaged, the modal displacement at the corresponding points of the damage location increases relatively, leading to changes in the BMC. Therefore, an indicator γ_i^r referred as to ACBMC is established to describe the differences to identify the damaged edge, as follows:

$$\gamma_i^r = \frac{\left(\left\{C_i^r\right\}_d^T \left\{C_i^r\right\}_u\right)^2}{\left(\left\{C_i^r\right\}_d^T \left\{C_i^r\right\}_d\right)\left(\left\{C_i^r\right\}_u^T \left\{C_i^r\right\}_u\right)} \tag{3}$$

where $\left\{C_i^r\right\}$ is the BMC for mode i and edge r. Subscripts u and d represent an undamaged and damaged edge, respectively. The ACBMC decreases with the increase in the damage severity of the edge r. Therefore, the damaged edge can be identified by the ACBMC.

2.3. Second Stage on Structural Sealant Damage Localization

After the damaged edge is identified in the first stage, the exact damage location of structural sealant can be further identified in the second stage. According to the changes in BMC caused by damage, the difference in the BMC $D_{j,i}^r$ can be defined as follows:

$$D_{j,i}^r = \left| \frac{\left(C_{j,i}^r\right)_u - \left(C_{j,i}^r\right)_d}{\left(C_{j,i}^r\right)_u} \right| \tag{4}$$

Since the structural sealant is an elastic boundary and affected by spring support, when local damage occurs to the structural sealant, the closer to the damage location, the bigger the changes in the BMC. Due to the influence of noise, there are also certain differences in the BMC obtained from the actual testing. The differences in the BMC caused by noise can be considered to follow a normal distribution. Therefore, the characteristics of the normal distribution can be used to identify the damage location. For the damaged

edge, the average and standard variance of the difference in the BMC for each measured point can be expressed as

$$\overline{E}_i^r = \frac{1}{n_r}\sum_{j=1}^{n_r} D_{j,i}^r \tag{5}$$

$$\sigma_i^r = \sqrt{\frac{1}{n_r}\sum_{j=1}^{n_r}\left(D_{j,i}^r - \overline{E}_i^r\right)^2} \tag{6}$$

where $\overline{E}_i^r$ and σ_i^r are the average and the standard variance for mode i and edge r, respectively. At a certain confidence level α, the data judged as anomalous can be identified using [30], as follows:

$$D_{j,i}^r \le \overline{E}_i^r - z\frac{\sigma_i^r}{\sqrt{n_r}} \text{ or } D_{j,i}^r \ge \overline{E}_i^r + z\frac{\sigma_i^r}{\sqrt{n_r}} \tag{7}$$

where z is quantile, usually 1.645. When $D_{j,i}^r$ satisfies Equation (7), the point-j of the edge-r is identified as the damage location.

To clearly describe the two-stage damage location identification method, Figure 2 illustrates the basic steps of the two-stage identification method. Firstly, the damaged edges are identified in the first stage; then, the specific damage location are identified based on the difference in ACBMC in the second stage.

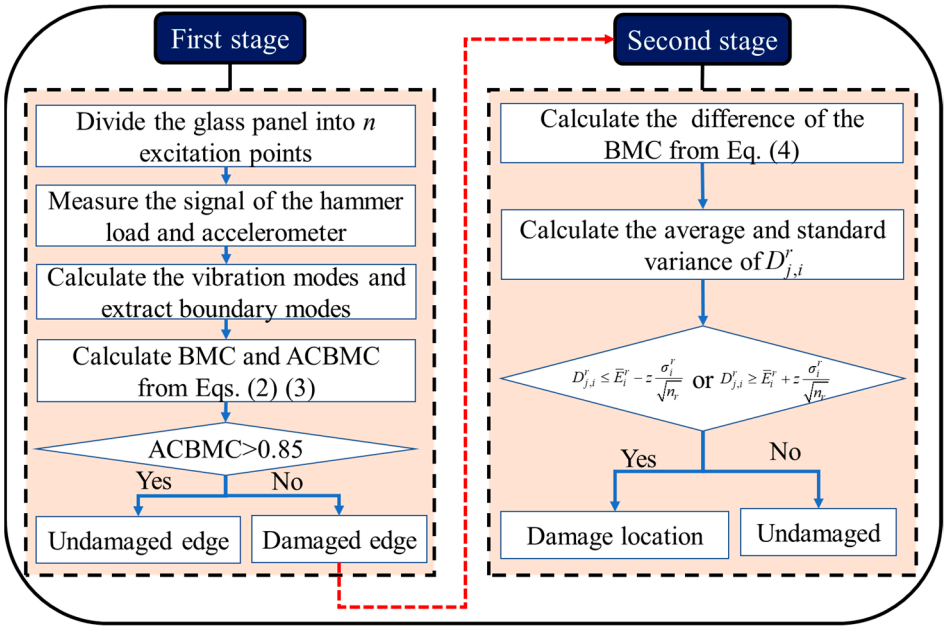


Figure 2. The flow chart of the proposed two-stage method.

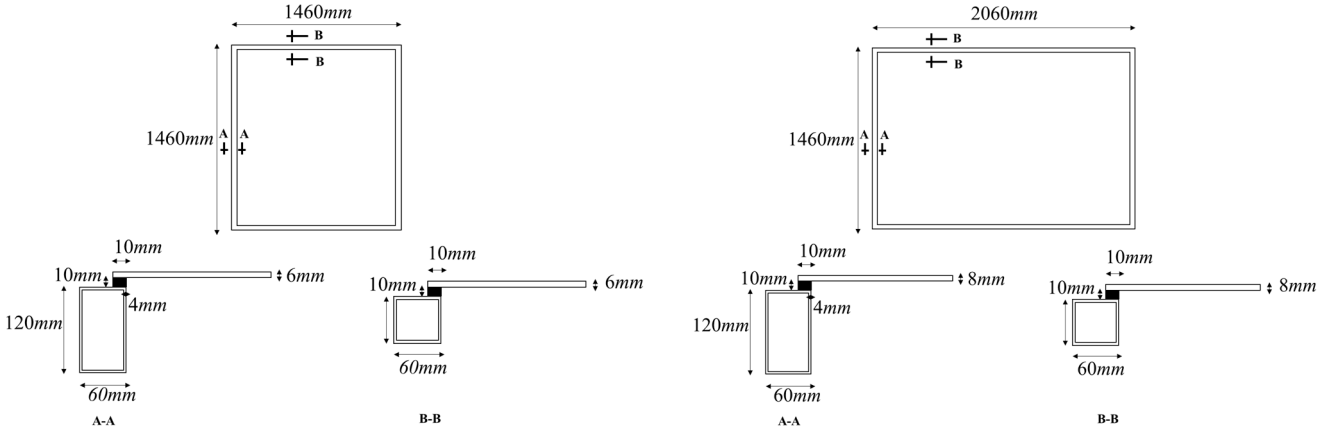
3. Numerical Validation

To validate the effectiveness of the proposed method, two numerical models were established in this section, and the boundary modes of the structural sealant under different damage scenarios are analyzed to identify the damage location in the structural sealant.

3.1. The Numerical Models

Figure 3 shows two full-sized panel units. The glass panels in Model A and Model B are 1460 mm and 2060 mm in width, 6 mm and 8 mm in thickness, and both 1410 mm in height, respectively. These panels are bonded to the frame with structural sealant with a width of 10 mm and a thickness of 10 mm. The supporting frame of the two samples adopts an aluminum alloy box section. The cross section size of the column frame is

60 mm × 120 mm and the wall thickness is 4 mm. The cross section size of the beam is 60 mm × 60 mm and the wall thickness is 4 mm.



(**a**) (**b**)

Figure 3. Dimensions of panel units design drawing: (**a**) Model-A and (**b**) Model-B.

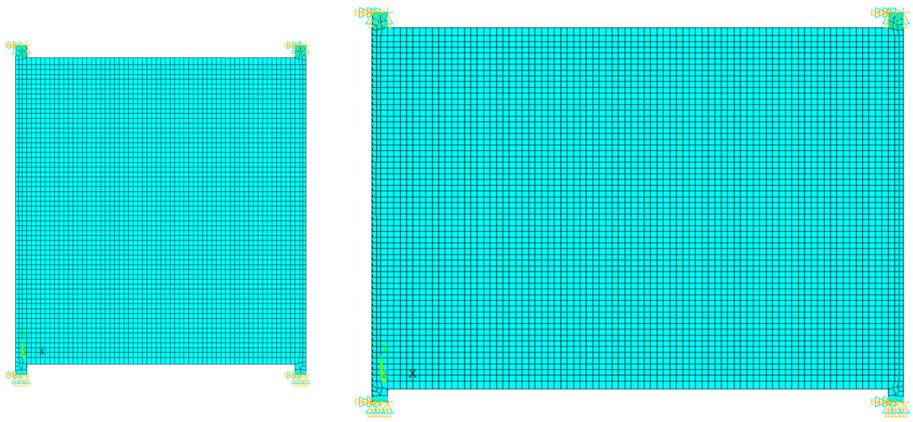
Table 1 lists the mechanical parameters of the materials. In the finite element models, the glass panel and supporting frame were meshed using shell elements. The element size was set as 0.025 m. The structural sealant was modeled with spring elements, and the stiffness per unit length is given by

$$k = \frac{E_s w_s}{t_s} \tag{8}$$

where E_s is the elastic modulus of structural sealant and w_s and t_s are the width and thickness of the structural sealant, respectively. The four corners of the supporting frame are fixed constraints. The two finite element models are shown in Figure 4.

Table 1. Mechanical parameters of the materials.

Materials	Density (kg/m^3)	Elastic Modulus (N/mm^2)	Poisson's Ratio
Glass panel	2500	7.0×10^4	0.22
Sealant	1350	1.12 (20 °C)	0.45
Supporting frame	2800	7×10^4	0.33



(**a**) (**b**)

Figure 4. Finite element models: (**a**) Model-A and (**b**) Model-B.

Mode analysis was performed to obtain the natural frequencies and associated mode shapes. Practical measurements would include noise, so random numbers were added to the calculated mode displacements, as follows:

$$\varphi_{j,i}{}^{s} = \varphi_{j,i} + \delta(2R - 1)\varphi_{j,i} \tag{9}$$

where $\varphi_{j,i}$ is the calculated mode displacement for mode i and point j, $\varphi_{j,i}{}^{s}$ is the mode displacement added noise, δ is noise level, and R is a random number of uniform distribution in the interval [0, 1]. In this study, a level of 5% noise was considered.

3.2. Damage Cases

As shown in Figures 5 and 6, the four edges of the finite element models are labeled as a, b, c, and d. The damage to the structural sealant was simulated by removing the spring elements that connected to the edge of the glass panel and the supporting frame. To describe the testing situation more intuitively, the measurement points on each edge are numbered in turn, as shown in Figures 5 and 6, which is consistent with the number of the spring unit.

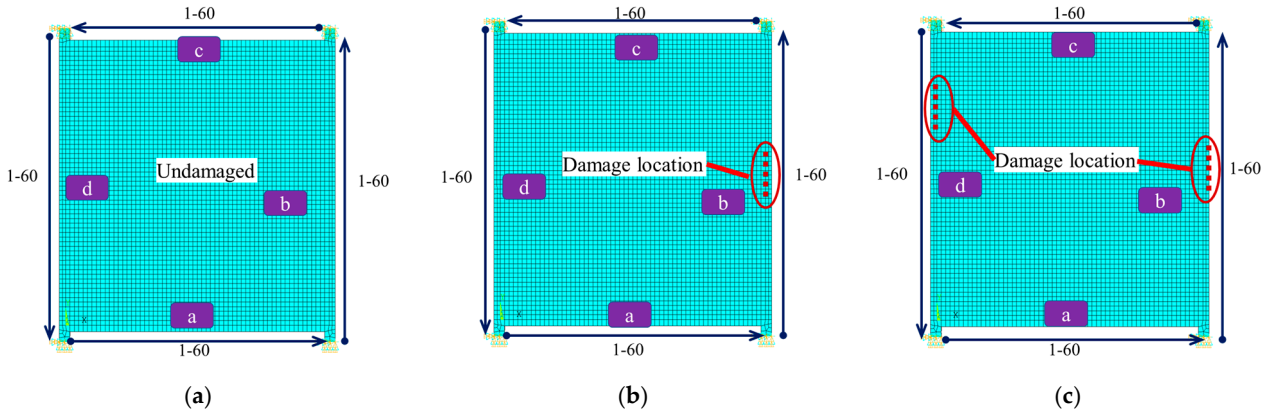


Figure 5. Damage cases of model A (**a**) Case 1, (**b**) Case 2–5, (**c**) Case 6–9.

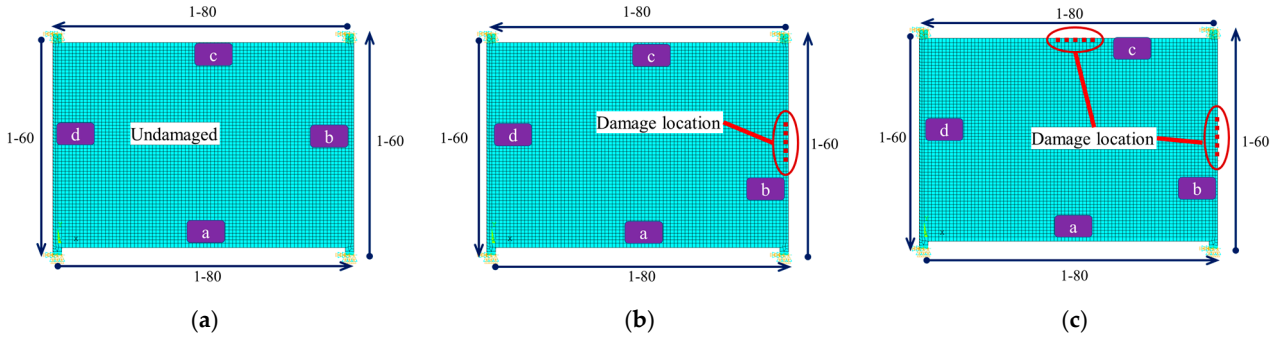


Figure 6. Damage cases of model B (**a**) Case 1, (**b**) Case 2–5, (**c**) Case 6–9.

Each edge's points are numbered sequentially, and the damage cases for both models are listed in Table 2. Additionally, the corresponding damage severities are list in the Table 2. As the damage location area increases, the damage severity gradually increases. The numbers in each cases represent the point ranges corresponding to the damage location of the structural sealant. There are four single-edge damage cases and four two-edge damage cases for both models. Figures 5 and 6 show the schematics of these damage cases.

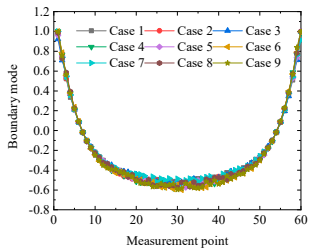
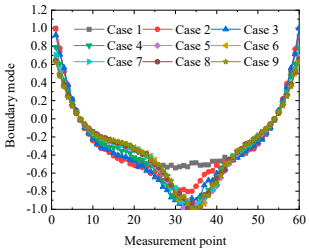
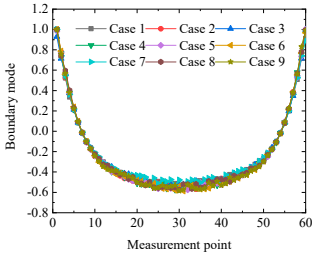
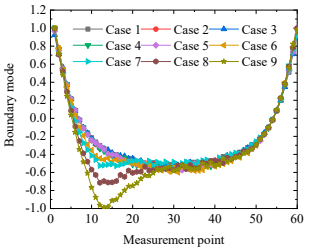
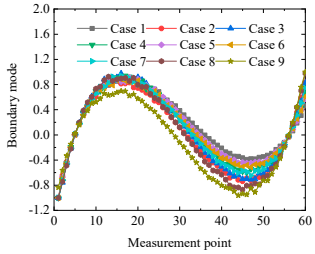
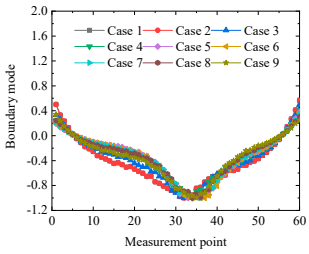
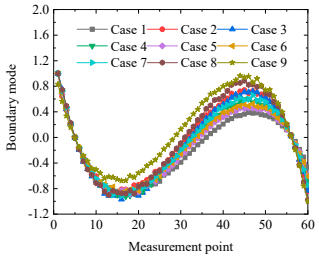
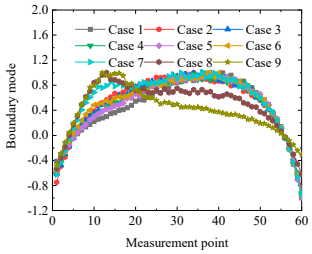
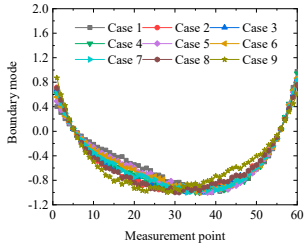
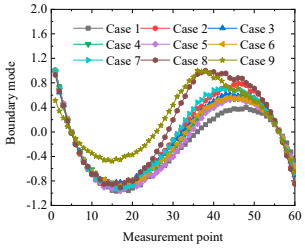
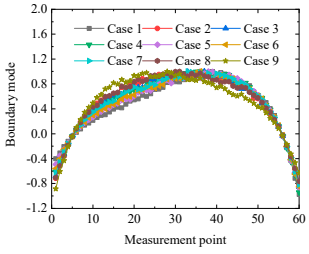
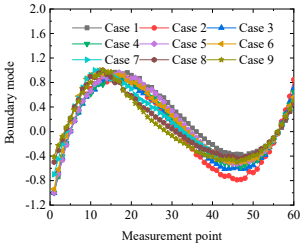
Table 2. Location and length of damage points.

Model	Edge	Damage	Case								
			1	**2**	**3**	**4**	**5**	**6**	**7**	**8**	**9**
A	E_b	Location	-	30–32	30–34	30–36	30–38	30–38	30–38	30–38	30–38
		Severity	0	5%	8.3%	11.6%	15%	15%	15%	15%	15%
	E_d	Location	-	-	-	-	-	10–12	10–14	10–16	10–18
		Severity	0	0	0	0	0	5%	8.3%	11.6%	15%
B	E_b	Location	-	28–30	28–32	28–34	28–36	28–36	28–36	28–36	28–36
		Severity	0	5%	8.3%	11.6%	15%	15%	15%	15%	15%
	E_c	Location	-	-	-	-	-	38–40	38–42	38–44	38–46
		Severity	0	0	0	0	0	3.8%	6.3%	8.8%	11.3%

3.3. Numerical Results

Table 3 lists the first three boundary modes of the nine cases of Model A. Significant changes in boundary modes are observed with damage in the structural sealant. For case 2–5, the first boundary mode of edge-b changes significantly as damage severity increases, while the boundary modes of undamaged edges-a, c, and d remain mostly unchanged. In cases 6–9, damage on edge-d causes notable displacement increases. For example, in cases 6 and 9, the displacement of edge-d increases by 7.6% and 50%, respectively, compared to the undamaged case. However, the displacement changes on edges-a and c are minimal.

Table 3. Boundary modes of Model A.

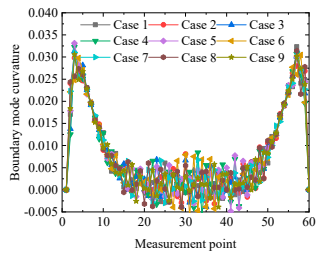
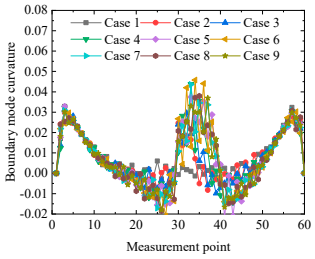
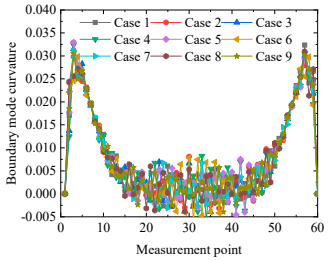
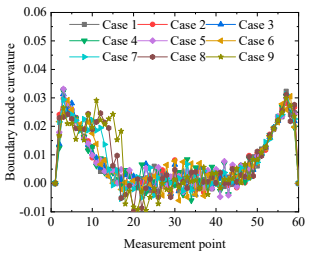
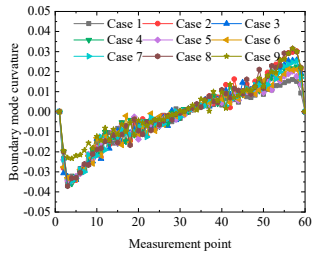
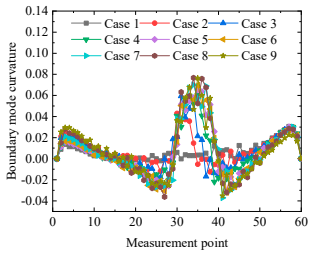
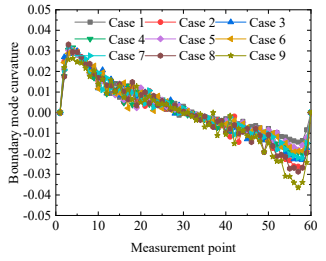
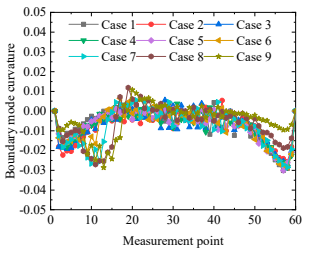
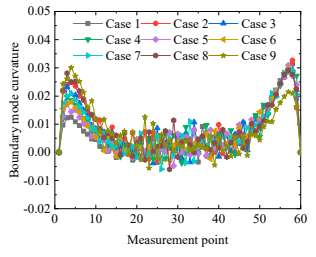
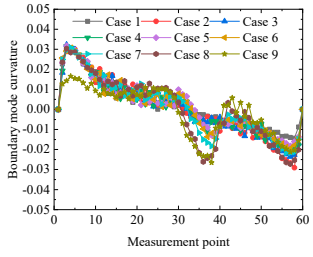
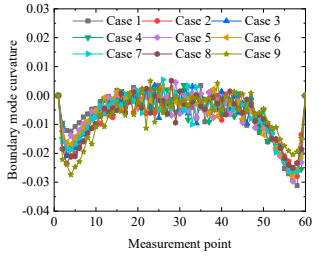
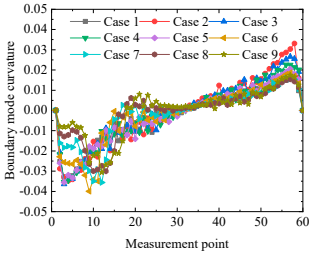
Mode	Edge a	Edge b	Edge c	Edge d
1st				
2nd				
3rd				

Interestingly, the second and third boundary modes of undamaged edges-a and c change significantly with increasing damage severity on edges-b and d. For the damaged edge b and d, the higher boundary modes are not always changed with the increase in the

damage severity, for instance, the second boundary mode of edge-b and the third boundary mode of edge-d. This can be attributed to two reasons: (1) higher boundary modes are more sensitive to local damage and when adjacent edges are damaged, the boundary modes of undamaged edges may also change. (2) When the damage is located at the modal node position, the boundary modes will not change regardless of the extent of the damage.

Table 4 lists the first three BMCs for Model A. Due to the influence of noise, the BMC shows some discreteness, and the same situation will occur in the actual measurement. In this case, the influence of noise can be reduced by averaging multiple measurements. Compared with boundary modes, the BMC is more sensitive to the damage. In the first-order boundary mode, the BMC of edge-b at the damage location is more than 10 times larger than that at non-damage. As the damage severity increases, the BMC at the damage location increases significantly, while the BMC at the undamaged location shows minimal change. Therefore, damage can be better identified by the changes in BMC. The results for Model B are similar and will not be repeated here.

Table 4. BMC of Model A.

BMC	Edge a	Edge b	Edge c	Edge d
1st				
2nd				
3rd				

3.3.1. Identification of the Damaged Edge

Figures 7 and 8 show the ACBMC of each edge calculated by Equation (3). The BMAC [29] is also shown for comparison. For the first boundary mode, the ACBMC of undamaged edges-a and c in Model A and edges-a and d in Model B do not show significant changes, remaining above 0.85. Conversely, the ACBMC of damaged edges drops below 0.85. Therefore, the ACBMC of the first mode can be used to identify the damaged edges. The threshold of the ACBMC of the first mode can be set as 0.85 for damaged edge identification.

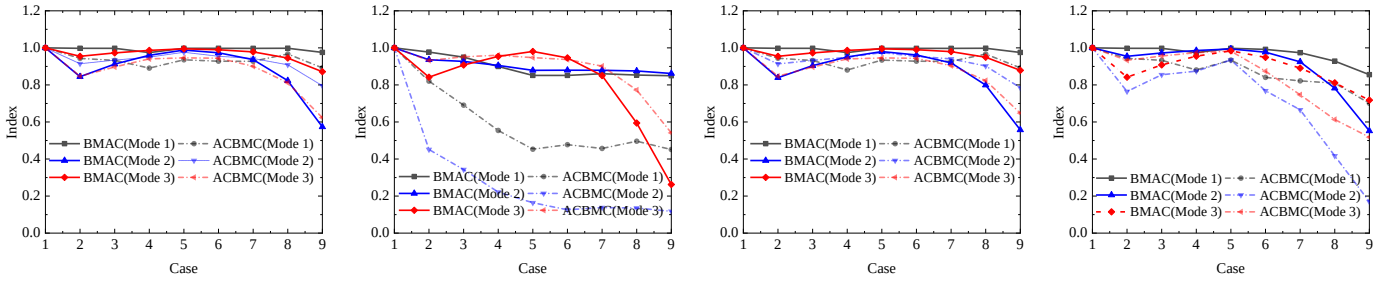


Figure 7. ACBMC and BMAC of model-A (**a**) Edge a, (**b**) Edge b, (**c**) Edge c, (**d**) Edge d.

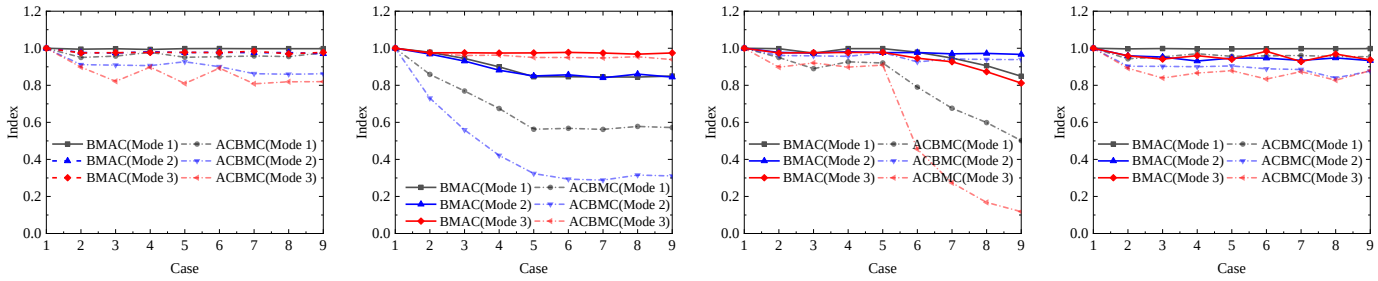


Figure 8. ACBMC and BMAC of model-B (**a**) Edge a, (**b**) Edge b, (**c**) Edge c, (**d**) Edge d.

In the second and third modes, the ACBMC of undamaged edges tends to decrease as damage severity increases. For example, the ACBMC of the second mode of the edge-d shows a significant decrease in cases 2–5. Additionally, the ACBMC of undamaged edges sometimes shows significant decreases or increases. Thus, the first mode's ACBMC is more reliable for damaged edge identification.

At the same time, it can also be observed that the change in the BMAC is less than the ACBMC when the damage severity is increased. This indicates that the ACBMC is more suitable for damage identification of structural sealant than the BMAC.

In the first stage of identification, the ACBMC of all edges is 1 in case 1; therefore, all of the edges are undamaged. In cases 2–5, the ACBMC of the first mode of edge-b are 0.82, 0.69, 0.55, and 0.45, respectively, which are less than 0.85. Therefore, the edge b can be identified as the damaged edge. The ACBMC of the first mode of edges a, c, and d are all higher than 0.85, so the three edges are undamaged. At this time, BMAC is 0.97, 0.94, 0.89, and 0.85, respectively. Compared with ACBMC, the changes in BMAC are relatively small and not sensitive to damage, so it is difficult to identify damage through changes in BMAC. In cases 6–9, the ACBMC of edges a and c are both higher than 0.85. The ACBMC of the first mode of edge-b and d are both less than 0.85. The damaged edges of model B can also be identified by the ACBMC. Therefore, using the ACBMC of the first mode to identify the damaged edge is consistent with the real damage cases.

3.3.2. Identification of the Damage Location

Once the damaged edge is identified, the damage location can be further identified in the second stage. Figure 9 shows the difference in the BMC $D^r_{j,1}$ for the first mode. It can be seen that there are many local peaks in $D^r_{j,1}$ due to the effect of noise, but significant increases in $D^r_{j,1}$ indicate damage. The average and standard deviation of $D^r_{j,1}$ of edges b and d were calculated according to Equations (5) and (6). Then, the damage location can be identified by Equation (7). Table 5 lists the identified damage location. By comparing Tables 2 and 5, it can be found that these locations closely match the actual damage positions. The identified damaged range is a little less than the actual one. The reason is that the

abnormal difference in the BMC would be found by Equation (7). $D^r_{j,1}$ is the most obvious at the central range of damage location, which is easy to identify.

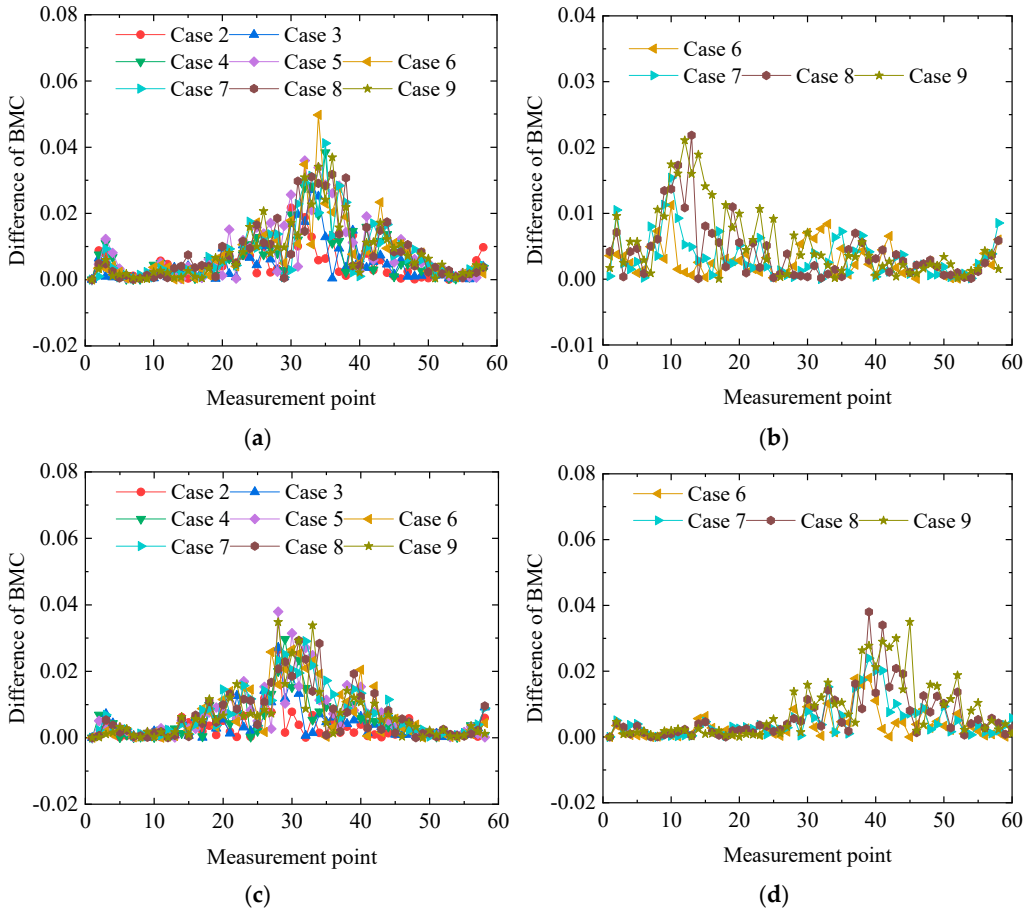


Figure 9. DBMC of model A and model B (**a**) Edge b (model-A), (**b**) Edge d (model-A), (**c**) Edge b (Model-B), (**d**) Edge c (Model-B).

Table 5. The identified damaged points of model A and B.

Model	Edge	Case							
		2	**3**	**4**	**5**	**6**	**7**	**8**	**9**
A	E_b	30–32	31–33	31–33	32–33	32–33	32–33	32–33	32–33
	E_d	-	-	-	-	9–11	10–12	12–13	12–14
B	E_b	28–29	28–29	29–30	31–32	31–32	32–34	32–33	32–33
	E_c	-	-	-	-	37–39	38–39	39–41	39–41

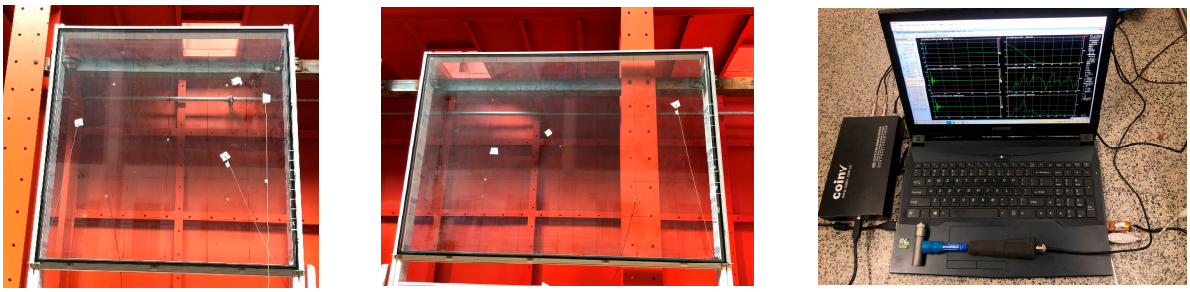
Based on the above results, it can be found that the precise identified damage location is related to the number of measurement points on each edge of the glass panel. Usually, the damage location can be identified at different numbers of measurement points. However, there are differences in the identified location. As the number of measurement points increases, the identified location would be more accurate. In typical experiments, more than five measurement points are set on each edge. Therefore, further research is needed to determine the optimal number of measurement points.

4. Test Validation

4.1. Modal Experiment

According to the actual service status of HFGCW, two full-size panel units, referred as specimen-A and specimen-B, were constructed in the laboratory, as shown in Figure 10.

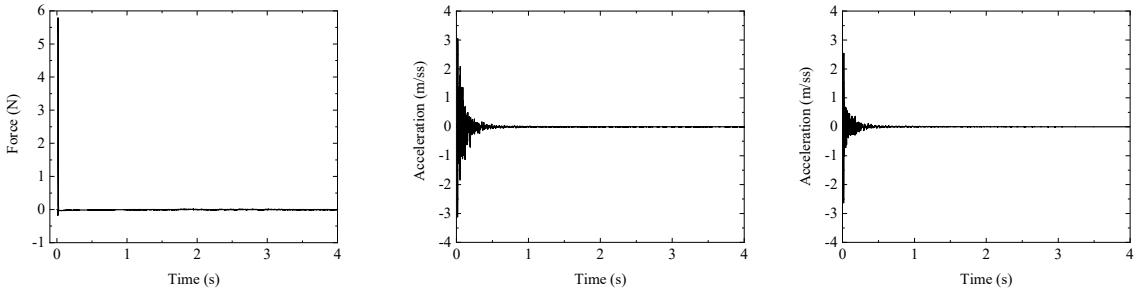
The dimensions of these models match those used in the numerical simulations, as shown earlier in Figure 3. The structural sealant was filled and cured for three months, ensuring that the structural sealant was completely cured and undamaged.



(**a**) (**b**) (**c**)

Figure 10. Test models (**a**) specimen-A, (**b**) specimen-B, (**c**) data acquisition and hammer.

The modes of panel units were identified through the ERA method [31,32]. In the hammer testing, multiple input multiple output (MIMO) was used. The glass panels of specimens-A and B were divided into 49 and 63 excitation points, respectively. In specimen-A, the acceleration sensors were installed at points 25 and 33 on the glass panel. In specimen-B, the acceleration sensors were installed at points 32 and 43. The sampling frequency and duration were set as 2048 and 4 s. The force hammer and acceleration sensor were supplied by Dytran Instruments, Inc. (Los Angeles, CA, USA) (Force hammer: Dytran-5800B4; Acceleration sensor: Dytran-3097A2, sensitivity range of ±100 mV/g). The weight of the sensor is 4.3 g, which is much less than the weight of the glass panel unit, so the sensor mass is ignored. The portable data collection instrument was provided by China Orient Institute of Noise & Vibration Coinv (3018A) (Beijing, China), as shown in Figure 10c. In order to compare the characteristics of the spectrum, the original acceleration response of the quarter intersection of the long and short sides on the glass panel was also measured and shown in the Figure 11.



(**a**) (**b**) (**c**)

Figure 11. Testing signal of two models (**a**) hammer signal, (**b**) acceleration signal (specimen—A), (**c**) acceleration signal (specimen—B).

4.2. Setting of the Damage Cases

To replicate structural sealant damage, the sealant was partially cut around the panel edges. The damage severity d_s was defined as the ratio of the cutting structural sealant length l_d to the total length l_t, as follows:

$$d_s = \frac{l_d}{l_t} \times 100\% \tag{10}$$

To realize the local damage in practical engineering, different damage severities were set, ranging from 0% to 8%. The damage was divided into 9 cases, and the damage severity of each case was expanded by 1%. The edge-b was the damaged edge, and the edge a, c

and d were undamaged edges, as shown in Figure 12. Table 6 lists the locations of damaged points and the corresponding different damage cases.

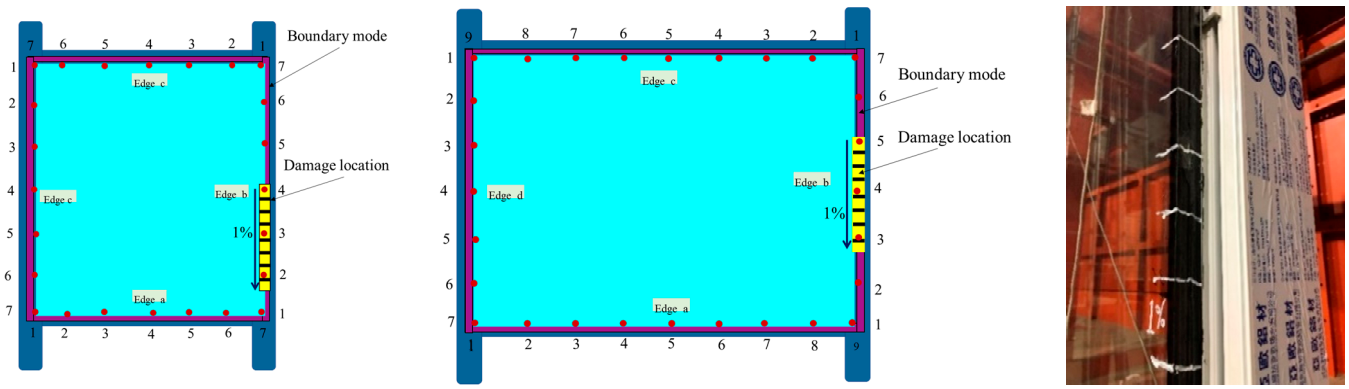


Figure 12. Testing model (**a**) specimen—A, (**b**) specimen—B, (**c**) damage setting.

Table 6. Actual damaged edge and damage points.

Specimen	Damaged Edge	Case								
		1	2	3	4	5	6	7	8	9
A	b	No damage	4	4	4	3–4	3–4	3–4	2–4	2–4
B	b	No damage	5	5	5	4–5	4–5	4–5	3–5	3–5

4.3. Experimental Results and Discussion

According to the experimental results, the first boundary modes of specimen-A were extracted as shown in Figure 13. In the undamaged edge, the modal displacements showed minimal differences, while the damaged edge (edge-b) exhibited significant displacement variations at points 2 and 3. Due to the symmetry effect, the difference between the boundary modes at point 5 was also generated. Figure 14 shows the BMC. It can be clearly seen that the difference between the BMC gradually increases with the increase in damage severity. In the damaged range of edge-b, the BMC of case 7 was twice as large as that of the undamaged area. Similar trends were observed in specimen-B, and hence, the results are not repeated.

In the current study, frequency spectrum methods are often used for damage identification. Figure 15 shows the spectrum of the fundamental frequencies of the two models. According to the calculation results of finite element model, it can be seen that the actual measured spectrum is relatively close to the calculated spectrum, but there are little differences. Because of the effect of model damping and actual manufacturing or construction errors, it is difficult for the finite element model and the actual model to accurately correspond. Therefore, the frequency and spectrum methods can be used as an auxiliary method.

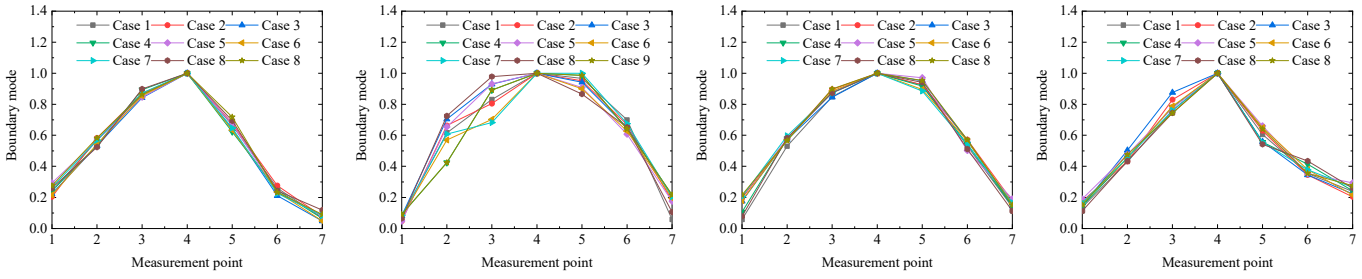


Figure 13. Boundary mode of specimen-A (**a**) Edge a, (**b**) Edge b, (**c**) Edge c, (**d**) Edge d.

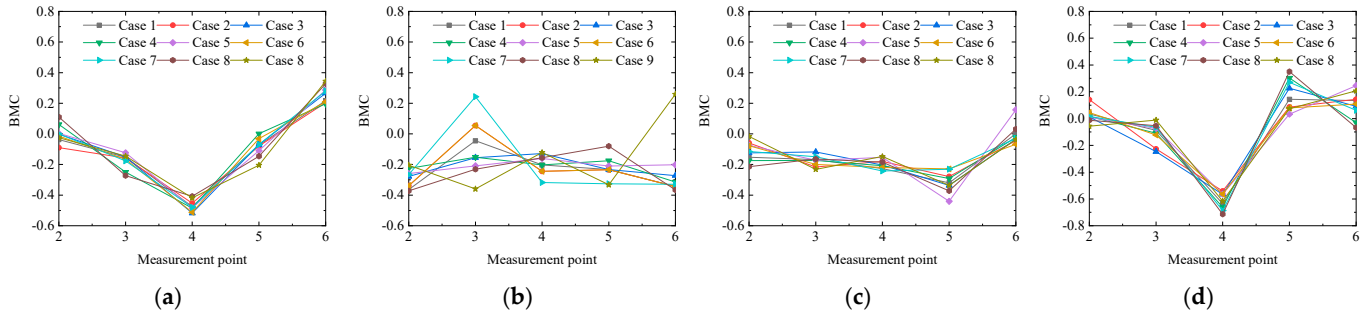


Figure 14. BMC of specimen-A (**a**) Edge a, (**b**) Edge b, (**c**) Edge c, (**d**) Edge d.

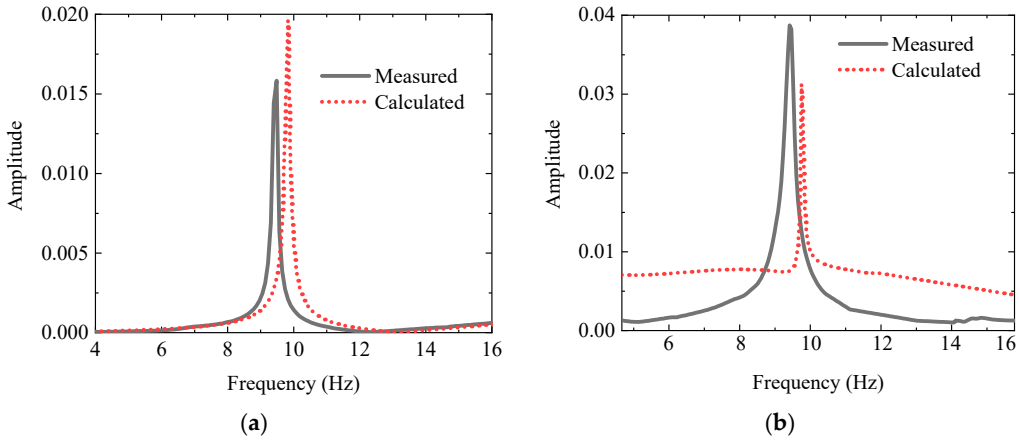


Figure 15. Measured spectra and calculated spectra (**a**) specimen—A, (**b**) specimen—B.

4.3.1. Identification in the First Stage

In the first stage, the ACBMC was used to identify the damaged edges. The ACBMC of each edge of specimen-A and B are shown in Figure 16. In case 1, all ACBMC were 1; they indicate that the edges were undamaged. In specimen-A, the damage severity of cases 2–4 was small; the ACBMC of all edges remained above 0.85, and it is difficult to identify the damaged edges. After the case 5, the damage severity was higher than 4%, the ACBMC of edge-b started to decrease significantly, reaching values of 0.84 and 0.65 in Cases 5 and 9, respectively. They were identified as the damaged edge. Other edges remained undamaged, with ACBMC values consistently above 0.85. The change laws of ACBMC of specimen-B were consistent with specimen-A. In cases 1–4, the damaged edge was not identified; in cases 5–9, the edge-b were identified as the damaged edge.

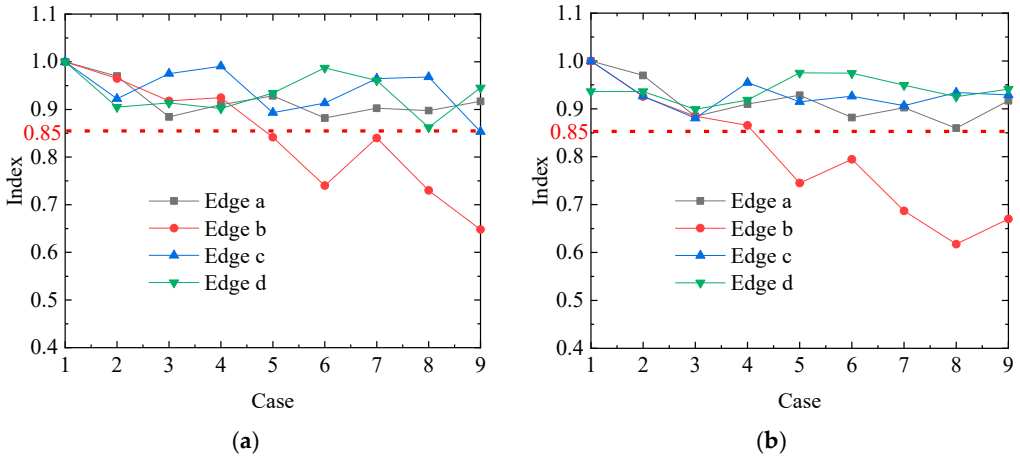


Figure 16. The ACBMC of two models (**a**) specimen-A, (**b**) specimen-B.

4.3.2. Identification in the Second Stage

According to the identification results of the first stage, the difference in the BMC of edge-b was calculated, as shown in Figure 17. In specimen-A, measured point 3 on edge-b showed a significant difference from other points. Similarly, in specimen-B, point 4 on edge-b exhibited a prominent BMC difference. The average and standard deviation of difference in the BMC for two models were calculated; then, the damage locations were identified according to Equation (7). The results are listed in Table 7.

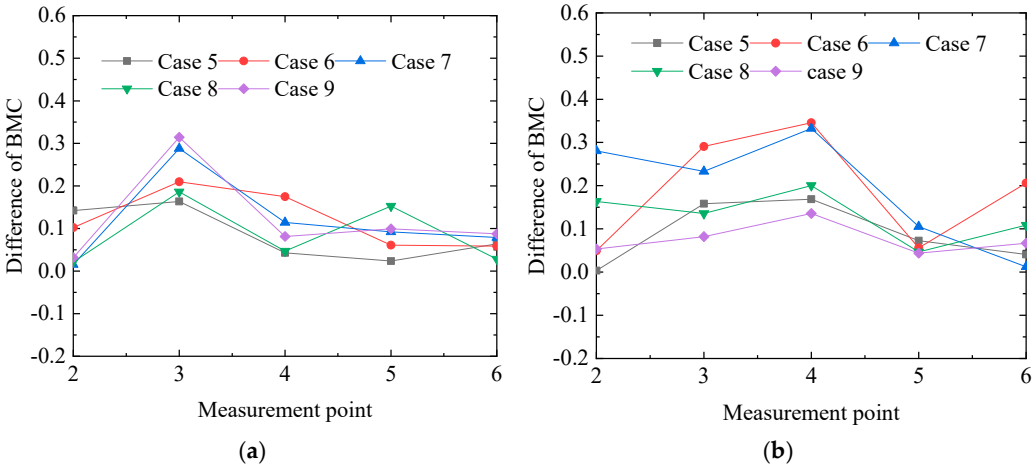


Figure 17. The difference in the BMC (**a**) Edge b (specimen-A), (**b**) Edge b (specimen-B).

Table 7. Identified damaged location of specimen-A and B.

Specimen	Edge	Case				
		5	**6**	**7**	**8**	**9**
A	E_b	3	3	3	3	3
B	E_b	4	4	4	4	4

When the damage severity exceeded 4%, significant changes in boundary modes and BMC allowed for the exact identification of both the damaged edges and their specific locations. It should be pointed out that the damage location can be identified through the change in the curvature of the boundary modal displacement when the damage reaches a certain severity. Whereas, in other forms of the glass curtain wall, such as the point-supported or exposed frame-supported glass curtain wall, the minimum severity that can be identified will change and needs to be further verified by experiments.

5. Conclusions

In this paper, a two-stage damage localization method is proposed to identify the damaged edges and midpoints of damaged structural sealants through the BMC. Based on the numerical and experimental results, the following conclusions can be drawn:

(1) The damaged edges of the structural sealant can be identified by the proposed ACBMC index effectively. A threshold value of 0.85 for the ACBMC of the first mode can identify the damaged edges of the structural sealant. Through numerical calculations and actual experiments, it can be found that the ACBMC index is more sensitive to damage than BMC alone. Additionally, the change in the ACBMC of the first mode is consistent with the increase in the damage severity. Due to the nodes of higher-order modes and the effect of noise, second-order and third-order modes cannot be used for damage identification;

(2) After identifying the damaged edge, the specific damage location of the structural sealant can be further identified through the difference in BMC. Based on the assumption that the differences in the BMC caused by noise follow a normal distribution, the

midpoint of the damage location can be identified. As the number of measurement points increases, the identified location would be more accurate, but the required labor in actual engineering increases. Usually, the number of measurement points on single-edge must reach more than 5;

(3) The method can be affected by the damage severity and noise in actual use. When the damage severity is small or the noise is high, the accuracy of this method decreases. When the damage severity exceeds 4%, the two-stage damage localization method can effectively identify the midpoint of the actual damage range.

However, in this study, only the damage identification of the frame-supported panel unit was carried out. In the future, further research is needed to identify the damage of other forms of glass curtain walls. Because the damage location is random, the number of measurement points also needs to be further discussed.

Author Contributions: Conceptualization, D.P.; Methodology, X.Z., K.J. and D.P.; Formal analysis, K.J.; Investigation, K.J.; Resources, X.F. and N.H.; Writing—original draft, K.J.; Writing—review & editing, D.P. All authors have read and agreed to the published version of the manuscript.

Funding: This study was supported by the Opening Funds of the State Key Laboratory of Building Safety and Built Environment and National Engineering Research Center of Building Technology (No. BSBE2022-06). The support is gratefully acknowledged.

Institutional Review Board Statement: Not applicable.

Informed Consent Statement: Not applicable.

Data Availability Statement: The raw data supporting the conclusions of this article will be made available by the authors on request.

Conflicts of Interest: The authors declare that they have no known competing financial interests or personal relationships that could have appeared to influence the work reported in this paper.

References

1. Bedon, C.; Amadio, C. Numerical assessment of vibration control systems for multi-hazard design and mitigation of glass curtain walls. *J. Build. Eng.* **2018**, *15*, 1–13. [CrossRef]
2. Bedon, C.; Xihong, Z.; Filipe, H. Dániel. Performance of structural glass facades under extreme loads—Design methods, existing research, current issues and trends. *Constr. Build. Mater.* **2018**, *3*, 921–937. [CrossRef]
3. Carolina, A.; Nicola, C.; Giuseppe, M.; Bonati, A.; Franco, A. Experimental and numerical investigation of cyclic response of a glass curtain wall for seismic performance assessment. *Constr. Build. Mater.* **2018**, *187*, 596–609. [CrossRef]
4. Memari, A.; Chen, X.; Kremer, P.; Behr, R. Prediction of seismic failure of silicone sealant in two-edged structural sealant glazing systems. *J. Archit. Eng.* **2012**, *18*, 6–26. [CrossRef]
5. *JGJ 102-2010*; Technical Code for Glass Curtain Wall Engineering. Construction Industry Press: Beijing, China, 2010. (In Chinese)
6. *ASTM E283-04*; Standard Test Method for Determining Rale of Air Leakage Through Exterior Windows, Curtain Walls and Doors Under Specified Pressure Differences Across the Specimen. American Society of Testing Materials: West Conshohocken, PA, USA, 2013.
7. *ASTM E331*; Standard Test Method for Water Penetration of Exterior Windows, Skylights, Doors and Curtain Walls by Uniform Static Air Pressure Difference. American Society of Testing Materials: West Conshohocken, PA, USA, 2009.
8. *AAMA 503*; Voluntary Specification for Field Testing of Newly Installed Storefronts Curtain Walls and Sloped Glazing Systems. American Architectural Manufacturers Association: Schaumburg, IL, USA, 2014.
9. *EN 13830-2003*; Curtain Walling—Product Standard. CEN: Brussels, Belgium, 2014.
10. *EOTA, ETAG 002*; Guideline for European Technical Approval for Structural Sealant Glazing Systems. CEN: Brussels, Belgium, 2001.
11. Hong, X.; Yuan, L.; Lin, P. Interfacial Adhesion-Strength Detection of Structural Silicone Sealant for Hidden Frame-Supported Glass Curtain Wall Based on Nonlinear Ultrasonic Lamb Wave. *J. Aerosp. Eng.* **2018**, *31*, 4018047. [CrossRef]
12. Lin, J.; Hong, X.; Ren, Z.; Chen, J. Scanning laser in-depth heating infrared thermography for deep debonding of glass curtain walls structural adhesive. *Measurement* **2022**, *192*, 110902. [CrossRef]
13. Zhu, R.; Chen, Y.; Liu, J. Current situation of safety detection technology on existing glass curtain wall. *China Build. Mater. Technol.* **2018**, *27*, 1–3. (In Chinese)
14. Doebline, S.; Farrar, C.; Prime, M.; Shevitz, D. *Damage Identification and Health Monitoring of Structural and Mechanical Systems from Changes in the Vibration Characteristics: A Literature Review*; Los Alamos National Laboratory Report LA-13070-MS; Office of Scientific and Technical Information, U.S. Department of Energy: Way Oak Ridge, TN, USA, 1996; Volume 30, pp. 2043–2049. [CrossRef]

15. Mahmud, M.; Samman, A.; Mrinmay, B. Vibration testing for nondestructive evaluation of bridges. I: Theory. *J. Struct. Eng.* **1994**, *120*, 269–289. [CrossRef]
16. Huang, Z.; Xie, M.; Song, H.; Du, Y. Modal analysis related safety-state evaluation of hidden frame supported glass curtain wall. *J. Build. Eng.* **2018**, *2*, 671–678. [CrossRef]
17. Huang, Z.; Xie, M.; Zhao, J.; Du, Y. Rapid evaluation of hidden frame supported glass curtain wall safety state based on remote vibration measurement. *J. Build. Eng.* **2018**, *5*, 91–97. [CrossRef]
18. Huang, Z.; Xie, M.; Chen, C.; Du, Y.; Zhao, J. Engineering application of a safety-state evaluation model for hidden frame-supported glass curtain walls based on remote vibration. *J. Build. Eng.* **2019**, *8*, 100915. [CrossRef]
19. Pan, D.; Jiang, K.; Zhang, X.; Huang, Y. Sealants delamination detection of structural sealant glazing systems based on driving-point accelerance. *Shock Vib.* **2020**, *5*, 7260438. [CrossRef]
20. Jiang, K.; Pan, D.; Huang, Y.; Qiu, X. Construction defects identification for structural sealant by statistical driving-point accelerance. *Constr. Build. Mater.* **2023**, *392*, 131817. [CrossRef]
21. Yang, G.; Long, X.; Wang, X. Structural adhesive damage identification of glass curtain wall. *Nonlinear Dyn.* **2022**, *110*, 2573–2587. [CrossRef]
22. Xu, H.; Yang, J.; Wang, X. Application of back propagation neural network on debonding prediction of glass curtain walls with concealed frame. *J. Chin. Ceram. Soc.* **2019**, *47*, 1073–1079. (In Chinese) [CrossRef]
23. Zhang, Q.; Yang, J.; Wang, X. Intelligent identification of connection relaxation state of frame supported glass curtain walls based on structural response vector and support vector machine. *J. Silic.* **2020**, *48*, 1682–1688. (In Chinese)
24. Zhang, S.; Li, C.; Ye, W. Damage localization in plate-like structures using time-varying feature and one-dimensional convolutional neural network. *Mech. Syst. Signal Process.* **2021**, *147*, 107107. [CrossRef]
25. Zhang, Y.; Miyamori, Y.; Mikami, S.; Saito, T. Vibration-based structural state identification by a 1 dimensional convolutional neural network. *Comput.-Aided Civ. Infrastruct. Eng.* **2019**, *34*, 822–839. [CrossRef]
26. Liu, X.; Bao, Y.; Song, Y.; Qiu, Y. Safety evaluation of glass curtain walls by using dynamic method. *China Civ. Eng.* **2009**, *42*, 11–15. (In Chinese) [CrossRef]
27. Liu, X.; Bao, Y. Safety evaluation for frame supported glass curtain wall based on natural frequency change. *J. Shenyang Univ. Technol.* **2011**, *33*, 595–600. (In Chinese)
28. Fang, Z.; Luo, W. Research on damage detection of fully hidden frame glass curtain wall based on modal curvature. *Value Eng.* **2017**, *36*, 89–93. (In Chinese) [CrossRef]
29. Jiang, K.; Pan, D.; Zhang, X.; Hu, N. Experimental study on damage identification of structural sealant based on boundary mode. *Eng. Mech.* **2022**, *39*, 350–355. (In Chinese) [CrossRef]
30. Aguinis, H.; Gottfredson, R.; Joo, H. Best-practice recommendations for defining, identifying, and handling outliers. *Organ. Res. Methods* **2013**, *16*, 270–301. [CrossRef]
31. Juang, J.; Richard, S. An eigensystem realization algorithm for modal parameter identification and model reduction. *J. Guid. Control Dyn.* **1985**, *8*, 620–627. [CrossRef]
32. Yang, X.; Yi, T.; Qu, C.; Li, H.; Liu, H. Automated eigensystem realization algorithm for operational modal identification of bridge structures. *J. Aerosp. Eng.* **2019**, *32*, 04018148. [CrossRef]

Disclaimer/Publisher's Note: The statements, opinions and data contained in all publications are solely those of the individual author(s) and contributor(s) and not of MDPI and/or the editor(s). MDPI and/or the editor(s) disclaim responsibility for any injury to people or property resulting from any ideas, methods, instructions or products referred to in the content.